

*Supplementary Information for*

## **Location of dopant dictates proton coupled electron transfer pathway in vanadium-substituted polyoxotungstates**

Zhou Lu<sup>1</sup>, Mamta Dagar<sup>1</sup>, James R. McKone<sup>2</sup>, and Ellen M. Matson\*<sup>1</sup>

<sup>1</sup>Department of Chemistry, University of Rochester, Rochester NY, 14627 USA

<sup>2</sup>Departments of Chemical and Petroleum Engineering and Chemistry, University of Pittsburgh, Pittsburgh PA, 15260 USA

E.M.M.: [matson@chem.rochester.edu](mailto:matson@chem.rochester.edu)

## Table of Contents

<b>General Considerations and Physical Measurements.</b> .....	4
<b>Synthetic procedure.</b> .....	4
<b>Figure S1.</b> $^{51}\text{V}$ NMR spectra of (a) $\text{PV}_{\text{out}}\text{W}_{11}$ and (b) $\text{V}_{\text{in}}\text{W}_{12}$ . .....	6
<b>Figure S2.</b> $^1\text{H}$ NMR spectrum of $1e^- - \text{PV}_{\text{out}}\text{W}_{11}$ . .....	6
<b>Figure S3.</b> $^{31}\text{P}$ NMR spectrum of $1e^- - \text{PV}_{\text{out}}\text{W}_{11}$ . .....	6
<b>Figure S4.</b> $^{51}\text{V}$ NMR spectrum of $1e^- - \text{PV}_{\text{out}}\text{W}_{11}$ . .....	7
<b>Figure S5.</b> $^1\text{H}$ NMR spectrum of $1e^- / 1\text{H}^+ - \text{PV}_{\text{out}}\text{W}_{11}$ . .....	7
<b>Figure S6.</b> $^1\text{H}$ NMR spectrum of $1e^- - \text{V}_{\text{in}}\text{W}_{12}$ . .....	7
<b>Figure S7.</b> Cyclic voltammograms of 1 mM $\text{PV}_{\text{out}}\text{W}_{11}$ obtained in acetonitrile in the presence of 6 mM various organic acids with the scan rate of 100 mV/s, using 0.1 M $[\text{Bu}_4\text{N}]\text{PF}_6$ as the supporting electrolyte. Ferrocene is used for each measurement as the internal standard. The corresponding acids are listed in <b>Table S1</b> . The breaks in the CVs denote the separation of the V-based and W-based redox events. The rationale behind separating these redox peaks lies in our motivation to refine the consequence of H-atom uptake on each of these electrochemical signatures. ....	8
<b>Table S1.</b> $\text{p}K_{\text{a}}$ values of various organic acids in acetonitrile. ....	8
<b>Figure S8.</b> $^1\text{H}$ -NMR spectrum of $\text{PV}_{\text{out}}\text{W}_{11}$ after adding half equivalent of 5,10-dihydrophenazine ( $\text{H}_2\text{Phen}$ ), showing the complete conversion to phenazine. The blue circles represent the $[\text{Bu}_4\text{N}]^+$ cations in the cluster, the black triangles are diethyl ether, and the asterisk is the trace unidentified impurity. ....	9
<b>Figure S9.</b> Electronic absorption spectra of fully-oxidized cluster $\text{PV}_{\text{out}}\text{W}_{11}$ and after (red) chemical reduction by $[\text{Bu}_4\text{N}]\text{BH}_4$ or (blue) bulk electrolysis at $-0.5$ V. All spectra are recorded in MeCN at room temperature. ....	9
<b>Figure S10.</b> (a) Chronoamperometry (I-t) curve for bulk electrolysis of $\text{PV}_{\text{out}}\text{W}_{11}$ at the applied potential of $-0.5$ V. (b) Cyclic voltammogram of 1 mM $\text{PV}_{\text{out}}\text{W}_{11}$ after bulk electrolysis with the scan rate of 100 mV/s. ....	10
<b>Figure S11.</b> FT-IR spectra of (black) $1e^- - \text{PV}_{\text{out}}\text{W}_{11}$ , and (red) $1e^- - \text{V}_{\text{in}}\text{W}_{12}$ . ....	11
<b>Figure S12.</b> FT-IR spectrum of $1e^- / 1\text{H}^+ - \text{PV}_{\text{out}}\text{W}_{11}$ with inset zoom-in figure to highlight the O–H vibration. ....	11
<b>Figure S13.</b> (Black) Experimental and (red) simulated electronic paramagnetic resonance (EPR) spectra of $1e^- - \text{PV}_{\text{out}}\text{W}_{11}$ . Simulation parameters: $g = [1.96666, 1.96942, 1.91502]$ ; $g$ -strain = $[0.0100439, 0.0102156]$ ; Hyperfine tensor = $[166.761, 177.671, 500.301]$ . ....	12
<b>Figure S14.</b> (Black) Experimental and (red) simulated electronic paramagnetic resonance (EPR) spectra of $1e^- / 1\text{H}^+ - \text{PV}_{\text{out}}\text{W}_{11}$ . Simulation parameters: $g = [1.96909, 1.96967, 1.91366]$ ; $g$ -strain = $[0.01139688, 0.0163894]$ ; Hyperfine tensor = $[183.444, 171.169, 509.709]$ . ....	12
<b>Figure S15.</b> Open circuit potential (OCP) measurements for the cluster pair of $\text{PV}_{\text{out}}\text{W}_{11}$ and $1e^- / 1\text{H}^+ - \text{PV}_{\text{out}}\text{W}_{11}$ using a three-electrode set-up with glassy carbon working electrode, Pt counter electrode, and Ag/AgNO <sub>3</sub> reference electrode in MeCN with 50 mM 4-methoxypyridine/4-methoxypyridium tetrafluoroborate (4-MeO-Pyr/4-MeO-PyrH <sup>+</sup> ) buffer and 0.1 M $[\text{Bu}_4\text{N}]\text{PF}_6$ supporting electrolyte. Three traces represent three independent measurements. The measurement is pre-equilibrated in the presence of 0.5 mM cluster 1 and 0.25 mM cluster 2; each step represents the injection of 100 $\mu\text{L}$ 2.5 mM cluster 2 stock solution. For black and blue traces, $1e^- / 1\text{H}^+ - \text{PV}_{\text{out}}\text{W}_{11}$ is cluster 1; for red trace, $\text{PV}_{\text{out}}\text{W}_{11}$ is cluster 1. ....	12
<b>Figure S16.</b> Plots of the OCP values referenced against H <sub>2</sub> measured at various concentration ratios of $1e^- / 1\text{H}^+ - \text{PV}_{\text{out}}\text{W}_{11}$ and $\text{PV}_{\text{out}}\text{W}_{11}$ versus the log of ratio of respective concentrations. The slope for the linear regression ( $\sim 0.059$ V/deg) closely resembles to Nernstian relation for a $1e^- / 1\text{H}^+$ process. The errors in average slope, $E^\circ_{\text{X}/\text{XH}_n}$ , and resulting BDFE(O–H) are from the standard errors obtained from three parallel experiments. ....	13
<b>Figure S17.</b> Electronic absorption spectra of 0.5 mM $\text{PV}_{\text{out}}\text{W}_{11}$ after adding half equivalent of $\text{H}_2\text{Phen}$ . 13	
<b>Figure S18.</b> Normalized absorbance trace over time of 0.25 mM $\text{PV}_{\text{out}}\text{W}_{11}$ after the addition of 2.5 mM (green) $\text{H}_2\text{Phen}$ or (orange) $\text{H}_2\text{Azo}$ at $-30$ °C. The monitored wavelengths are 424 and 370 nm for the	

addition of H<sub>2</sub>Phen and H<sub>2</sub>Azo, respectively. The discrepancy in the absorbance change of **PV<sub>out</sub>W<sub>11</sub>** towards H<sub>2</sub>Phen and H<sub>2</sub>Azo originates from the different monitored wavelengths to avoid the overlapped absorption. The full electronic absorption spectra are shown in Figure 5a, S24. .... 14

**Figure S19.** <sup>1</sup>H-NMR spectrum of **PV<sub>out</sub>W<sub>11</sub>** after adding half equivalent of hydrazobenzene (H<sub>2</sub>azo), showing the complete conversion to azobenzene. The blue circles represent the [<sup>n</sup>Bu<sub>4</sub>N]<sup>+</sup> cations in the cluster, the black triangles are diethyl ether, and the asterisk is the trace unidentified impurity. .... 14

**Figure S20.** Plot of absorbance at 370 nm over time for the reactions between 0.25 mM **PV<sub>out</sub>W<sub>11</sub>** and 2.5 mM H<sub>2</sub>Azo under pseudo-1<sup>st</sup>-order condition in MeCN at -30 °C with (gray) raw data and (red) fitting curve, along with fir-derived *k<sub>obs</sub>* and R<sup>2</sup> parameters. .... 14

**Figure S21.** Plot of absorbance at 370 nm over time for the reactions between 0.25 mM **PV<sub>out</sub>W<sub>11</sub>** and 3 mM H<sub>2</sub>Azo under pseudo-1<sup>st</sup>-order condition in MeCN at -30 °C with (gray) raw data and (red) fitting curve, along with fir-derived *k<sub>obs</sub>* and R<sup>2</sup> parameters. .... 15

**Figure S22.** Plot of absorbance at 370 nm over time for the reactions between 0.25 mM **PV<sub>out</sub>W<sub>11</sub>** and 4 mM H<sub>2</sub>Azo under pseudo-1<sup>st</sup>-order condition in MeCN at -30 °C with (gray) raw data and (red) fitting curve, along with fir-derived *k<sub>obs</sub>* and R<sup>2</sup> parameters. .... 15

**Figure S23.** Plot of absorbance at 370 nm over time for the reactions between 0.25 mM **PV<sub>out</sub>W<sub>11</sub>** and 5 mM H<sub>2</sub>Azo under pseudo-1<sup>st</sup>-order condition in MeCN at -30 °C with (gray) raw data and (red) fitting curve, along with fir-derived *k<sub>obs</sub>* and R<sup>2</sup> parameters. .... 15

**Figure S24.** Plot of absorbance at 370 nm over time for the reactions between 0.25 mM **PV<sub>out</sub>W<sub>11</sub>** and 2.5 mM H<sub>2</sub>Azo under pseudo-1<sup>st</sup>-order condition in MeCN at -20 °C with (gray) raw data and (red) fitting curve, along with fir-derived *k<sub>obs</sub>* and R<sup>2</sup> parameters. .... 15

**Figure S25.** Plot of absorbance at 370 nm over time for the reactions between 0.25 mM **PV<sub>out</sub>W<sub>11</sub>** and 2.5 mM H<sub>2</sub>Azo under pseudo-1<sup>st</sup>-order condition in MeCN at -10 °C with (gray) raw data and (red) fitting curve, along with fir-derived *k<sub>obs</sub>* and R<sup>2</sup> parameters. .... 16

**Figure S26.** Plot of absorbance at 370 nm over time for the reactions between 0.25 mM **PV<sub>out</sub>W<sub>11</sub>** and 2.5 mM H<sub>2</sub>Azo under pseudo-1<sup>st</sup>-order condition in MeCN at 0 °C with (gray) raw data and (red) fitting curve, along with fir-derived *k<sub>obs</sub>* and R<sup>2</sup> parameters. .... 16

**Figure S27.** Electronic absorption spectra of (blue) 0.1 mM 2,4,6-<sup>t</sup>Bu<sub>3</sub>PhO<sup>•</sup> radical in acetonitrile and (yellow) after the addition of one equivalent of **1e<sup>-</sup>/1H<sup>+</sup>-PV<sub>out</sub>W<sub>11</sub>**, showing the disappearance of 2,4,6-<sup>t</sup>Bu<sub>3</sub>PhO<sup>•</sup> radical and emergence of fully-oxidized **PV<sub>out</sub>W<sub>11</sub>**. .... 17

**Figure S28.** NMR spectrum of stoichiometric mixture of 2,4,6-<sup>t</sup>Bu<sub>3</sub>PhO<sup>•</sup> radical and **1e<sup>-</sup>/1H<sup>+</sup>-PV<sub>out</sub>W<sub>11</sub>** in CD<sub>3</sub>CN, showing the existence of -OH signal of 2,4,6-<sup>t</sup>Bu<sub>3</sub>PhOH. .... 17

**Figure S29.** Cyclic voltammograms of 1 mM **V<sub>in</sub>W<sub>12</sub>** obtained in acetonitrile in the presence of 4 mM various organic acids with the scan rate of 100 mV/s, using 0.1 M [<sup>n</sup>Bu<sub>4</sub>N]PF<sub>6</sub> as the supporting electrolyte. Ferrocene is used for each measurement as the internal standard. The corresponding acids are listed in **Table S1**. .... 18

**Figure S30.** Cyclic voltammograms of 1 mM 1,4-dihydroxynaphthalene (H<sub>2</sub>NQ) in acetonitrile with the scan rate of 100 mV/s, using 0.1 M [<sup>n</sup>Bu<sub>4</sub>N]PF<sub>6</sub> as the supporting electrolyte. .... 19

**Figure S31.** <sup>1</sup>H NMR spectra of the mixture of (upper) **V<sub>in</sub>W<sub>12</sub>** and half equivalent of 1,4-dihydroxynaphthalene (H<sub>2</sub>NQ) and (lower) **PV<sub>out</sub>W<sub>11</sub>** and H<sub>2</sub>NQ in CD<sub>3</sub>CN. The yellow- and green-shaded areas represent the H<sub>2</sub>NQ and dehydrogenated product 1,4-naphthoquinone (NQ), respectively. .... 19

**Figure S32.** Electronic absorption spectra of 0.5 mM **V<sub>in</sub>W<sub>12</sub>** after adding half equivalent of H<sub>2</sub>NQ. .... 20

**Figure S33.** Electronic absorption spectra of 0.5 mM **PV<sub>out</sub>W<sub>11</sub>** after adding half equivalent of H<sub>2</sub>NQ. .... 20

**Figure S34.** Illustration of atom numbers of **PV<sub>out</sub>W<sub>11</sub>** in conceptual density functional theory (CDFT) calculation. .... 21

**Table S2.** Conceptual density functional theory (CDFT) results for **PV<sub>out</sub>W<sub>11</sub>**. .... 22

**References**. .... 24

## General Considerations and Physical Measurements.

All experiments were carried out in a UniLab MBraun inert atmosphere glove box under a dinitrogen gas atmosphere. All glassware was oven-dried and cooled in an evacuated antechamber prior to use. Solvents were dried and deoxygenated on a glass contour system (Pure Process Technology, LLC) and stored over activated 3 Å molecular sieves.

Electronic absorption spectroscopy was recorded in dry acetonitrile in 1-cm-path quartz cuvettes with either Agilent Cary 60 UV-vis spectrophotometer or Agilent Cary 3500 Multicell UV-vis spectrophotometer. Elemental analysis was performed on a PerkinElmer 2400 Series II CHNS/O Elemental Analyzer. NMR studies were carried out on a Bruker 400 MHz or a Bruker 500 MHz spectrometer.  $^1\text{H}$  NMR was calibrated by using the solvent acetonitrile as 1.940 ppm;  $^{31}\text{P}$  and  $^{51}\text{V}$  NMR were externally calibrated by  $\text{H}_3\text{PO}_4$  and  $\text{VOCl}_3$ , respectively, as 0 ppm. All the NMR spectra were recorded in  $d_3$ -MeCN at room temperature unless specifically noted. Electron paramagnetic resonance (EPR) studies were performed on a Bruker EMXplus EPR spectrometer at 10 K using a J-Young EPR tube. EPR spectra were fitted and simulated by adopting the EasySpin toolbox (version 6.0.5).

All electrochemical studies were conducted on a BioLogic SP-150 Potentiostat in a  $\text{N}_2$ -filled glove box and acquired with the EC-Lab software (v11.42). Glassy carbon disc (3 mm, CH Instruments, USA) was used for cyclic voltammetry and open-circuit potential measurements as the working electrode, and a platinum mesh was used for bulk electrolysis as the working electrode. A nonaqueous  $\text{Ag}/\text{Ag}^+$  reference electrode with 100 mM  $[\text{Bu}_4\text{N}]\text{PF}_6$  and 10 mM  $\text{AgNO}_3$  solution in acetonitrile (BASi, USA) and a platinum wire were used as the reference and counter electrodes, respectively. All cyclic voltammetry (CV) analysis, open-circuit potential (OCP) measurements, and bulk electrolysis experiments were carried out at room temperature in acetonitrile and internally referenced to ferrocene ( $\text{Fc}^{+/0}$ ) redox couple, unless specifically noted.

**Kinetic analysis.** Pseudo-1<sup>st</sup>-order reaction conditions were used to find the rate expression for the reaction between  $[\text{Bu}_4\text{N}]_4[\text{PVW}_{11}\text{O}_{40}]$  ( $\text{PV}_{\text{out}}\text{W}_{11}$ ) and  $\text{H}_2\text{Azo}$ . The loss of absorbance at 370 nm of  $\text{PV}_{\text{out}}\text{W}_{11}$  was tracked to determine the rate expression,  $k_{\text{obs}}$ , over time, through the following Equation S1:

$$A_t = A_{\text{inf}} + (A_0 - A_{\text{inf}})e^{-k_{\text{obs}} \times t} \quad \text{Eqn. S1}$$

Where  $A_t$  is the absorbance at a given time,  $t$ , in seconds;  $A_{\text{inf}}$  is the absorbance at the end of the reaction ( $t = \text{infinite}$ );  $A_0$  is the absorbance at after organic PCET reagent injection; and  $k_{\text{obs}}$  is the observed 1<sup>st</sup>-order rate constant ( $\text{s}^{-1}$ ). Error was determined by calculating the standard deviation of  $k_{\text{obs}}$  between triplicate trials.

Eyring analysis was performed in the similar manner to find the rate expression at varied temperatures from  $-30$  to  $0$  °C with the constant concentrations of 0.25 mM for  $\text{PV}_{\text{out}}\text{W}_{11}$  and 2.5 mM for  $\text{H}_2\text{Azo}$ . Experiments were repeated in triplicate. The Eyring analysis results are plotted in  $\ln(k_{\text{obs}}/T)$  vs  $(1/T)$ , as follows in Equation S2. The Gibbs free energy is calculated by the following Equation S3.

$$\ln \frac{k_{\text{obs}}}{T} = \frac{-\Delta H^\ddagger}{R} \times \frac{1}{T} + \ln \frac{\kappa k_{\text{B}}}{h} + \frac{\Delta S^\ddagger}{R} \quad \text{Eqn. S2}$$

$$\Delta G^\ddagger = \Delta H^\ddagger - T\Delta S^\ddagger \quad \text{Eqn. S3}$$

Where  $T$  is the temperature in Kelvin,  $\Delta H^\ddagger$  is the enthalpy of activation,  $R$  is gas constant,  $\kappa$  is transmission coefficient,  $k_{\text{B}}$  is Boltzmann constant,  $h$  is Planck constant,  $\Delta S^\ddagger$  is the entropy of activation,  $\Delta G^\ddagger$  is the Gibbs free energy.

**Theoretical Considerations.** All the density functional theory (DFT) calculations were conducted by Gaussian 16 A.03 program package.<sup>1</sup> The initial guess of  $[\text{PV}_{\text{out}}\text{W}_{11}]$  was taken from the crystal structure MUWZIO by changing one W atom with V atom and removing all cations. The geometry was then optimized at the MN15/Def2-SVP level of theory and no imaginary frequencies were found to ensure the energy minima.<sup>2,3</sup> Single point calculations at the same level of theory were performed on  $N$ ,  $N+1$ ,  $N-1$  electron states of the cluster with respective (*charge, multiplicity*) combinations of  $(-4, 1)$ ,  $(-5, 2)$ ,  $(-3, 2)$ . Conceptual DFT (CDFT) calculations were conducted by Multiwfn 3.8(dev) software and adopting single point calculation output files with different electron states.<sup>4-6</sup>

## Synthetic procedure.

The syntheses of [<sup>n</sup>Bu<sub>4</sub>N]<sub>4</sub>[PV<sup>V</sup>W<sup>VI</sup><sub>11</sub>O<sub>40</sub>] (**PV<sub>out</sub>W<sub>11</sub>**) and [<sup>n</sup>Bu<sub>4</sub>N]<sub>3</sub>[V<sup>V</sup>W<sup>VI</sup><sub>12</sub>O<sub>40</sub>] (**V<sub>in</sub>W<sub>12</sub>**) adopted the procedure from ref. <sup>7,8</sup>.

**PV<sub>out</sub>W<sub>11</sub>**: <sup>1</sup>H NMR (400 MHz, CD<sub>3</sub>CN), δ = 3.15 (32H), 1.64 (32H), 1.40 (32H), 0.99 (48H). <sup>31</sup>P NMR (400 MHz, CD<sub>3</sub>CN), δ = -9.99 ppm. <sup>51</sup>V NMR (500 MHz, CD<sub>3</sub>CN), δ = -552.63 ppm.

**V<sub>in</sub>W<sub>12</sub>**: <sup>1</sup>H NMR (500 MHz, CD<sub>3</sub>CN), δ = 3.12 (24H), 1.63 (24H), 1.39 (24H), 0.99 (36H). <sup>51</sup>V NMR (500 MHz, CD<sub>3</sub>CN), δ = -579.12 ppm.

Synthesis of [<sup>n</sup>Bu<sub>4</sub>N]<sub>5</sub>[PV<sup>IV</sup>W<sup>VI</sup><sub>11</sub>O<sub>40</sub>] (**1e<sup>-</sup>-PV<sub>out</sub>W<sub>11</sub>**)

A 20-mL scintillation vial was charged with [<sup>n</sup>Bu<sub>4</sub>N]<sub>4</sub>[PV<sup>V</sup>W<sup>VI</sup><sub>11</sub>O<sub>40</sub>] (**PV<sub>out</sub>W<sub>11</sub>**, 0.100 g, 0.027 mmol) and [<sup>n</sup>Bu<sub>4</sub>N]BH<sub>4</sub> (0.0077 g, 0.030 mmol) dissolved in ~4 mL acetonitrile. The reaction mixture was stirred at 50 °C for >3 hrs to afford a deep purple solution. The solution was then concentrated under reduced pressure (~10 %), followed by washing with diethyl ether (5×3 mL). The purple powder was then filtered and dried under vacuum. Yield = 0.104 g, 97.9% based on **PV<sub>out</sub>W<sub>11</sub>**. <sup>1</sup>H NMR (400 MHz, CD<sub>3</sub>CN), δ = 3.18 (40H), 1.65 (40H), 1.41 (40H), 0.98 (60H). <sup>31</sup>P NMR (400 MHz, CD<sub>3</sub>CN), δ = -12.50 ppm. <sup>51</sup>V NMR (500 MHz, CD<sub>3</sub>CN), δ = -555.39 ppm. Anal. Calcd. for PVW<sub>11</sub>O<sub>40</sub>C<sub>80</sub>H<sub>180</sub>N<sub>5</sub>: C, 24.29%; H, 4.59%; N, 1.77%; found: C, 23.419%; H, 4.403%; N, 1.764%.

Synthesis of [<sup>n</sup>Bu<sub>4</sub>N]<sub>4</sub>[PV<sup>IV</sup>W<sup>VI</sup><sub>11</sub>(OH)O<sub>39</sub>] (**1e<sup>-</sup>/1H<sup>+</sup>-PV<sub>out</sub>W<sub>11</sub>**)

A 20-mL scintillation vial was charged with [<sup>n</sup>Bu<sub>4</sub>N]<sub>4</sub>[PV<sup>V</sup>W<sup>VI</sup><sub>12</sub>O<sub>40</sub>] (**PV<sub>out</sub>W<sub>11</sub>**, 0.100 g, 0.027 mmol) and hydrazobenzene (H<sub>2</sub>Azo, 0.003 g, 0.016 mmol) dissolved in ~4 mL acetonitrile. The reaction mixture was stirred at 50 °C for >2 hrs to afford a deep purple solution. The reaction mixture was then dried under reduced pressure, followed by washing with diethyl ether (3×6 mL) until colorless to remove residual azobenzene. The purple powder was then filtered and dried under vacuum. Yield = 0.949 g, 94.8% based on **PV<sub>out</sub>W<sub>11</sub>**. <sup>1</sup>H NMR (400 MHz, CD<sub>3</sub>CN), δ = 3.14 (32H), 1.64 (32H), 1.40 (32H), 0.99 (48H). Anal. Calcd. for PVW<sub>11</sub>O<sub>40</sub>C<sub>64</sub>H<sub>145</sub>N<sub>4</sub>: C, 20.69%; H, 3.93%; N, 1.51%; found: C, 20.516%; H, 3.714%; N, 1.362%.

Note: the usage of 5,10-dihydrophenazine (H<sub>2</sub>Phen) also leads to the formation of **1e<sup>-</sup>/1H<sup>+</sup>-PV<sub>out</sub>W<sub>11</sub>**; to push the reaction to completion, a slight overdose of H<sub>2</sub>Azo or H<sub>2</sub>Phen is adopted. The by-product from H<sub>2</sub>Azo is easy to remove by thoroughly washing with diethyl ether, while it is difficult to remove all the byproducts from H<sub>2</sub>Phen due to the solubility constraints. As such, we recommend using H<sub>2</sub>Azo as the H-atom donor for bulk synthesis.

Synthesis of [<sup>n</sup>Bu<sub>4</sub>N]<sub>4</sub>[V<sup>IV</sup>W<sup>VI</sup><sub>12</sub>O<sub>40</sub>] (**1e<sup>-</sup>-V<sub>in</sub>W<sub>12</sub>**).

The procedure is same as for **1e<sup>-</sup>-PV<sub>out</sub>W<sub>11</sub>**, except for the starting materials [<sup>n</sup>Bu<sub>4</sub>N]<sub>4</sub>[V<sup>V</sup>W<sup>VI</sup><sub>12</sub>O<sub>40</sub>] (**V<sub>in</sub>W<sub>12</sub>**, 0.100 g, 0.028 mmol) and [<sup>n</sup>Bu<sub>4</sub>N]BH<sub>4</sub> (0.0077 g, 0.030 mmol). The pale green powder was collected with the yield of 0.074 g, 69.4% based on **V<sub>in</sub>W<sub>12</sub>**. <sup>1</sup>H NMR (500 MHz, CD<sub>3</sub>CN), δ = 3.14 (32H), 1.64 (32H), 1.40 (32H), 0.99 (48H). Anal. Calcd. for VW<sub>12</sub>O<sub>40</sub>C<sub>64</sub>H<sub>144</sub>N<sub>4</sub>: C, 19.88%; H, 3.75%; N, 1.45%; found: C, 20.068%; H, 3.591%; N, 1.344%.

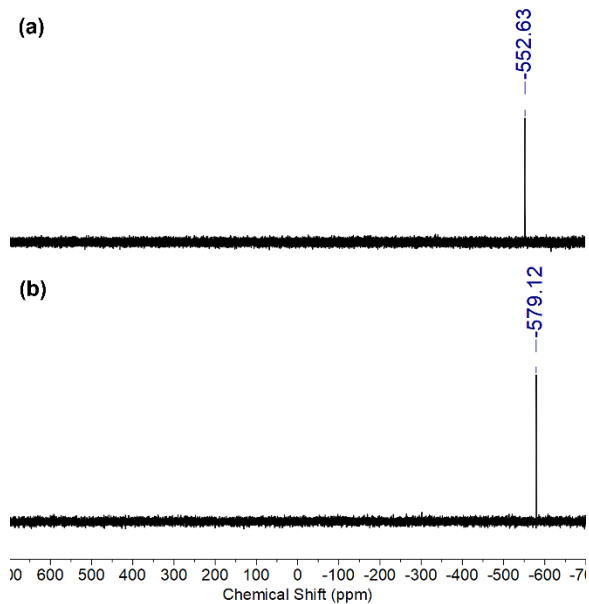


Figure S1.  $^{51}\text{V}$  NMR spectra of (a)  $\text{PV}_{\text{out}}\text{W}_{11}$  and (b)  $\text{V}_{\text{in}}\text{W}_{12}$ .

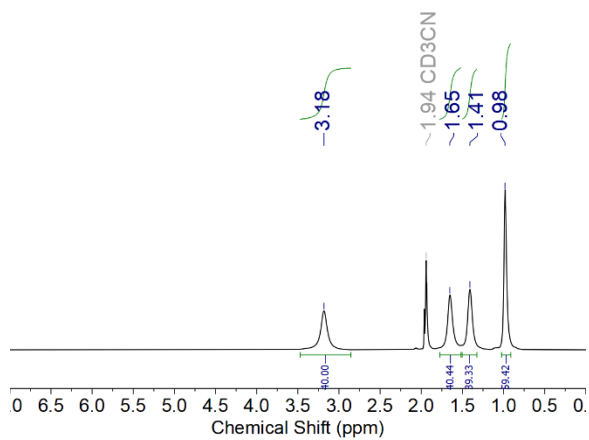


Figure S2.  $^1\text{H}$  NMR spectrum of  $1e^-$ - $\text{PV}_{\text{out}}\text{W}_{11}$ .

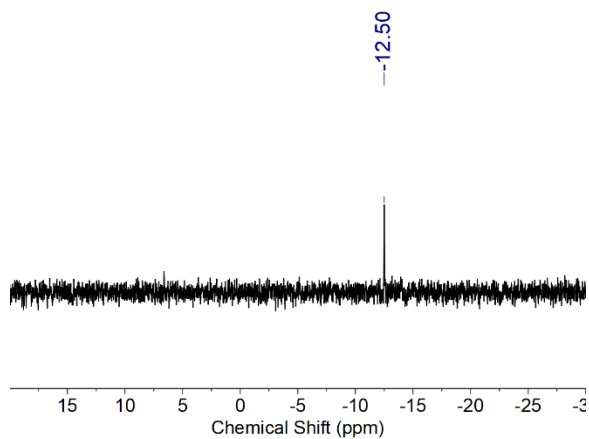


Figure S3.  $^{31}\text{P}$  NMR spectrum of  $1e^-$ - $\text{PV}_{\text{out}}\text{W}_{11}$ .

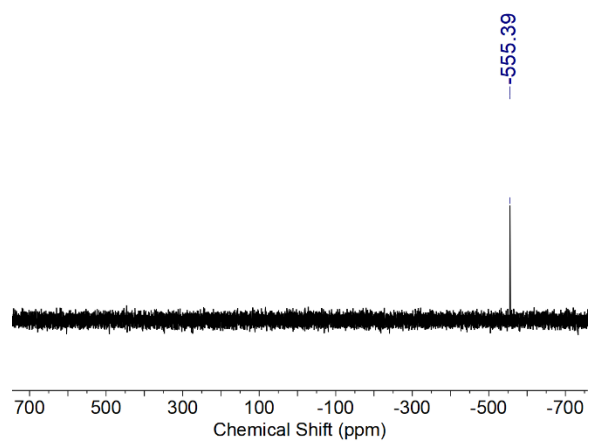


Figure S4.  $^{51}\text{V}$  NMR spectrum of  $1e^-$ -PV<sub>out</sub>W<sub>11</sub>.

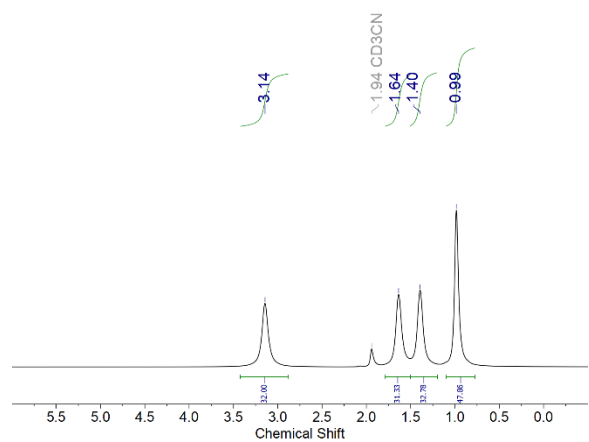


Figure S5.  $^1\text{H}$  NMR spectrum of  $1e^-/1\text{H}^+$ -PV<sub>out</sub>W<sub>11</sub>.

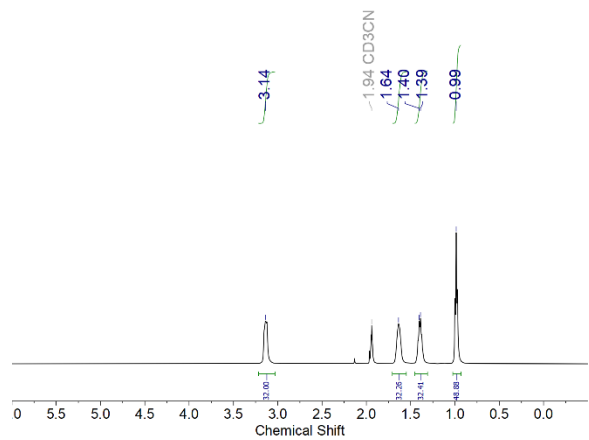
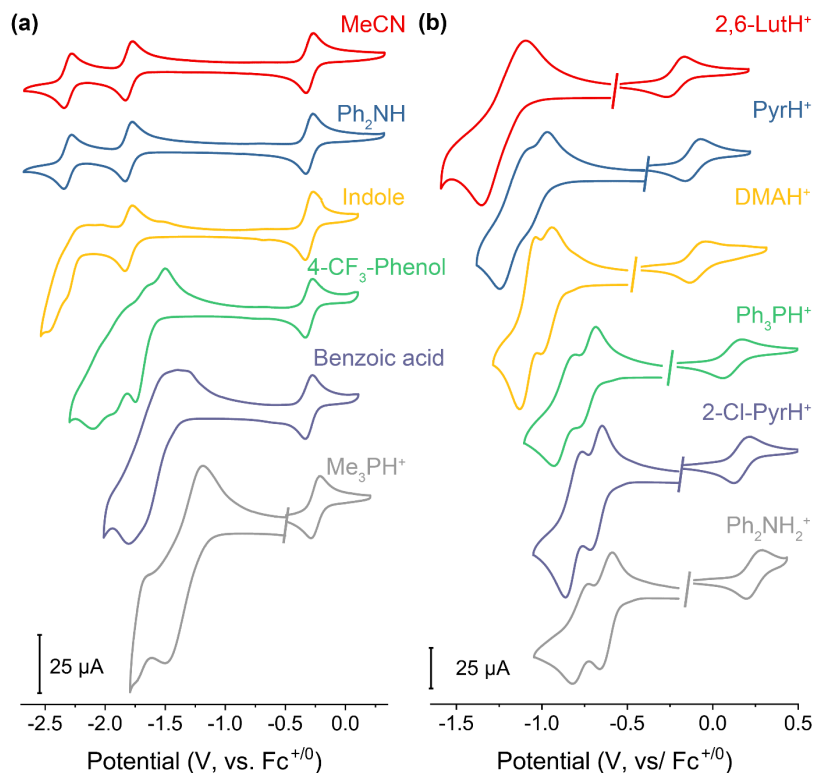


Figure S6.  $^1\text{H}$  NMR spectrum of  $1e^-$ -V<sub>in</sub>W<sub>12</sub>.



**Figure S7.** Cyclic voltammograms of 1 mM  $PV_{out}W_{11}$  obtained in acetonitrile in the presence of 6 mM various organic acids with the scan rate of 100 mV/s, using 0.1 M  $[nBu_4N]PF_6$  as the supporting electrolyte. Ferrocene is used for each measurement as the internal standard. The corresponding acids are listed in **Table S1**. The breaks in the CVs denote the separation of the V-based and W-based redox events. The rationale behind separating these redox peaks lies in our motivation to refine the consequence of H-atom uptake on each of these electrochemical signatures.

**Table S1.**  $pK_a$  values of various organic acids in acetonitrile.

Acid	Abbreviation	$pK_a(\text{MeCN})$	Ref.
Acetonitrile	MeCN	39.5	9,10
Diphenylamine	$Ph_2NH$	34.3	9,11
Indole		32.57	12
3-Trifluoromethyl-Phenol	3- $CF_3$ -phenol	26.5	12
4-Trifluoromethyl-Phenol	4- $CF_3$ -phenol	25.5	12
1,1,3,3-Tetramethylguanidinium tetrafluoroborate	$TMGH^+$	23.35	13
Benzoic acid		21.5	14
Trimethylammonium chloride	$Me_3NH^+$	17.61	13



Trimethylphosphonium tetrafluoroborate	$\text{Me}_3\text{PH}^+$	15.48	13
4-Methoxyl-Pyridium tetrafluoroborate	4-MeO-PyrH <sup>+</sup>	14.24	13
2,6-Lutidinium tetrafluoroborate	2,6-LutH <sup>+</sup>	14.16	13
Pyridium tetrafluoroborate	PyrH <sup>+</sup>	12.53	13
<i>N,N</i> -Dimethylanilinium tetrafluoroborate	DMAH <sup>+</sup>	11.47	13
Anilinium tetrafluoroborate	Anilinium <sup>+</sup>	10.64	13
Pyrazinium tetrafluoroborate	Pyrazinium <sup>+</sup>	7.74	13
2-Chloro-Pyridium tetrafluoroborate	2-Cl-PyrH <sup>+</sup>	6.79	13
Diphenylammonium tetrafluoroborate	$\text{Ph}_2\text{NH}_2^+$	5.98	13

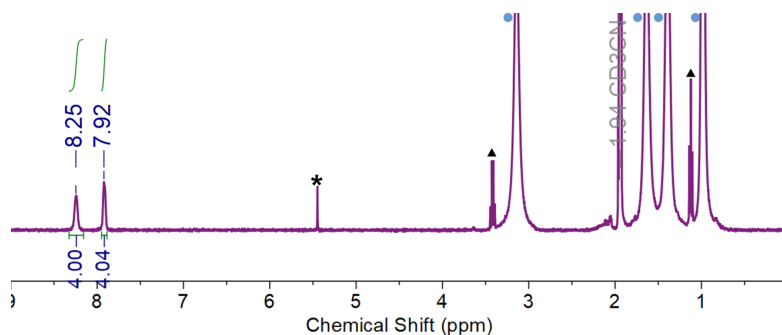


**Figure S8.** <sup>1</sup>H-NMR spectrum of  $\text{PV}_{\text{out}}\text{W}_{11}$  after adding half equivalent of 5,10-dihydrophenazine ( $\text{H}_2\text{Phen}$ ), showing the complete conversion to phenazine. The blue circles represent the  $[\text{Bu}_4\text{N}]^+$  cations in the cluster, the black triangles are diethyl ether, and the asterisk is the trace unidentified impurity.

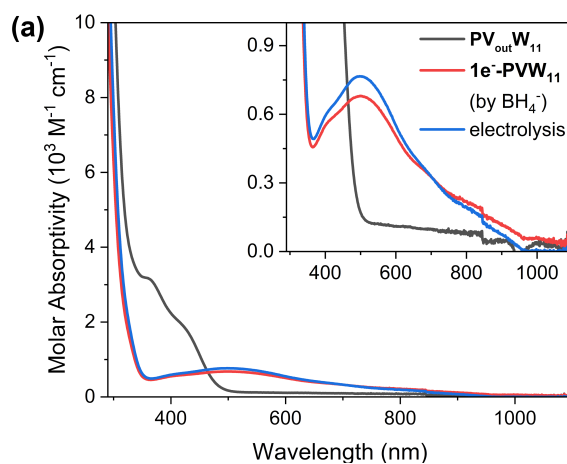


**Figure S9.** Electronic absorption spectra of fully-oxidized cluster  $\text{PV}_{\text{out}}\text{W}_{11}$  and after (red) chemical reduction by  $[\text{Bu}_4\text{N}]\text{BH}_4$  or (blue) bulk electrolysis at  $-0.5$  V. All spectra are recorded in MeCN at room temperature.

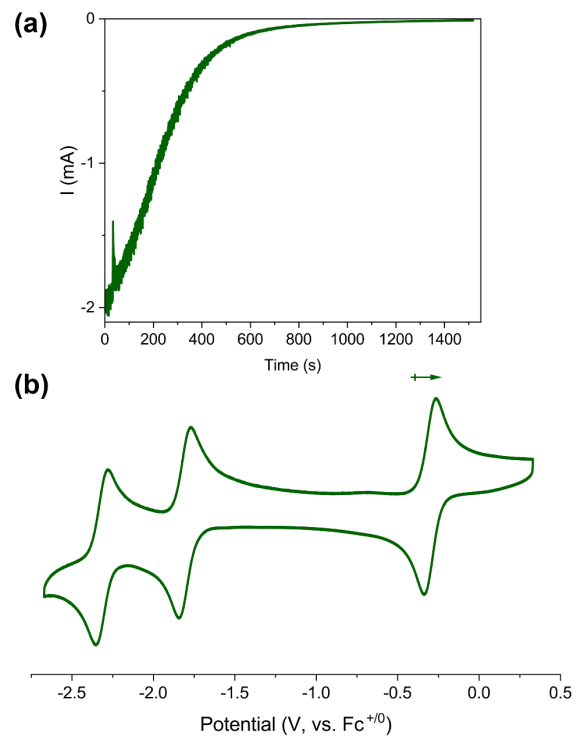


**Figure S10.** (a) Chronoamperometry (I-t) curve for bulk electrolysis of  $\text{PV}_{\text{out}}\text{W}_{11}$  at the applied potential of -0.5 V. (b) Cyclic voltammogram of 1 mM  $\text{PV}_{\text{out}}\text{W}_{11}$  after bulk electrolysis with the scan rate of 100 mV/s.

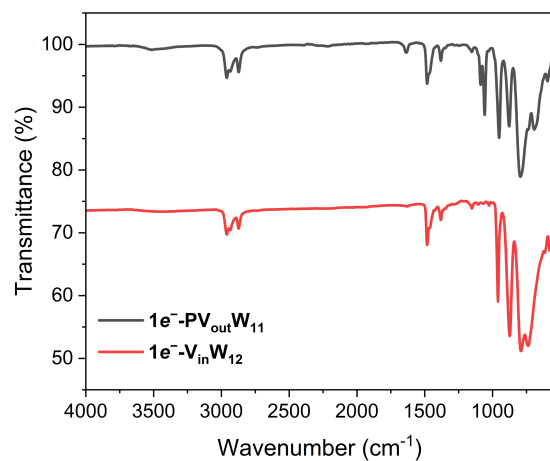


**Figure S11.** FT-IR spectra of (black)  $1e^-$ -PV<sub>out</sub>W<sub>11</sub>, and (red)  $1e^-$ -V<sub>in</sub>W<sub>12</sub>.

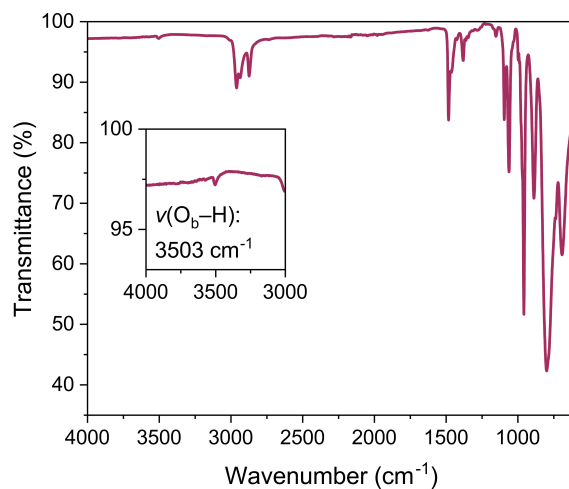


**Figure S12.** FT-IR spectrum of  $1e^-/1H^+$ -PV<sub>out</sub>W<sub>11</sub> with inset zoom-in figure to highlight the O–H vibration.

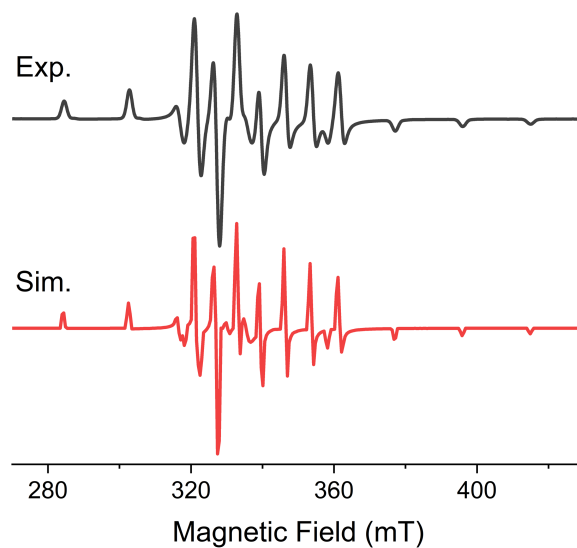


**Figure S13.** (Black) Experimental and (red) simulated electronic paramagnetic resonance (EPR) spectra of  $1e^-$ - $PV_{out}W_{11}$ . Simulation parameters:  $g = [1.96666, 1.96942, 1.91502]$ ;  $g$ -strain =  $[0.0100439, 0.0102156]$ ; Hyperfine tensor =  $[166.761, 177.671, 500.301]$ .

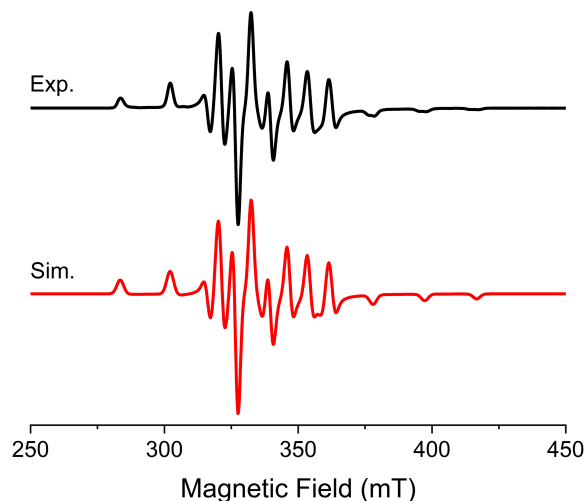


**Figure S14.** (Black) Experimental and (red) simulated electronic paramagnetic resonance (EPR) spectra of  $1e^-/1H^+$ - $PV_{out}W_{11}$ . Simulation parameters:  $g = [1.96909, 1.96967, 1.91366]$ ;  $g$ -strain =  $[0.01139688, 0.0163894]$ ; Hyperfine tensor =  $[183.444, 171.169, 509.709]$ .

Note: Comparing to the experimental EPR spectrum of  $1e^-$ - $PV_{out}W_{11}$ , it is noted that shoulder peaks exist with the hyperfine coupling peaks around 380 to 420 mT in  $1e^-/1H^+$ - $PV_{out}W_{11}$ . We attribute the existence of shoulder peaks to the partial electron delocalization over  $V^{IV}-O^b$  bond upon the protonation of bridging  $O^{2-}$  ligand.

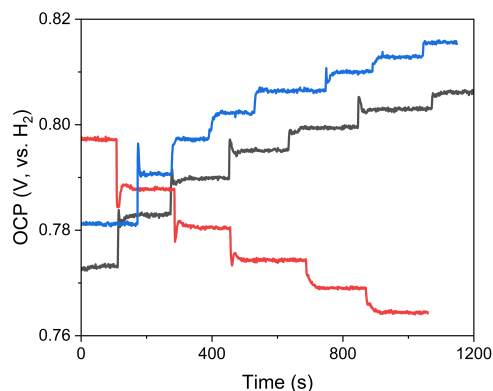


**Figure S15.** Open circuit potential (OCP) measurements for the cluster pair of  $PV_{out}W_{11}$  and  $1e^-/1H^+$ - $PV_{out}W_{11}$  using a three-electrode set-up with glassy carbon working electrode, Pt counter electrode, and  $Ag/AgNO_3$  reference electrode in MeCN with 50 mM 4-methoxypyridine/4-methoxypyridium tetrafluoroborate (4-MeO-Pyr/4-MeO-Pyr $H^+$ ) buffer and 0.1 M  $[nBu_4N]PF_6$  supporting electrolyte. Three traces represent three independent measurements. The measurement is pre-equilibrated in the presence of 0.5 mM cluster 1 and 0.25 mM cluster 2; each step represents the injection of 100  $\mu$ L 2.5 mM cluster 2 stock solution. For black and blue traces,  $1e^-/1H^+$ - $PV_{out}W_{11}$  is cluster 1; for red trace,  $PV_{out}W_{11}$  is cluster 1.

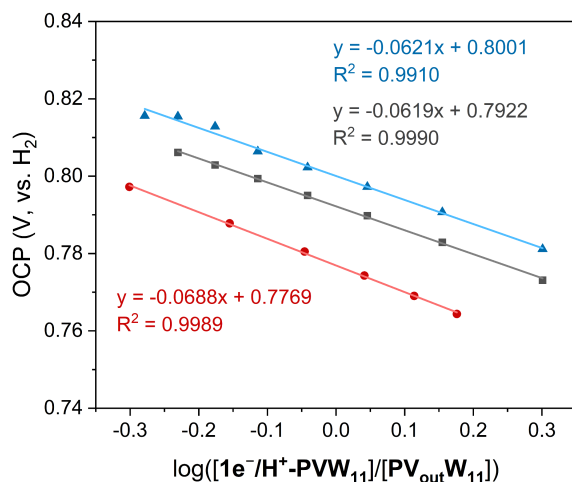


**Figure S16.** Plots of the OCP values referenced against  $H_2$  measured at various concentration ratios of  $1e^-/1H^+ - PV_{out}W_{11}$  and  $PV_{out}W_{11}$  versus the log of ratio of respective concentrations. The slope for the linear regression ( $\sim -0.059$  V/deg) closely resembles to Nernstian relation for a  $1e^-/1H^+$  process. The errors in average slope,  $E^\circ_{X/XH_n}$ , and resulting BDFE(O-H) are from the standard errors obtained from three parallel experiments.

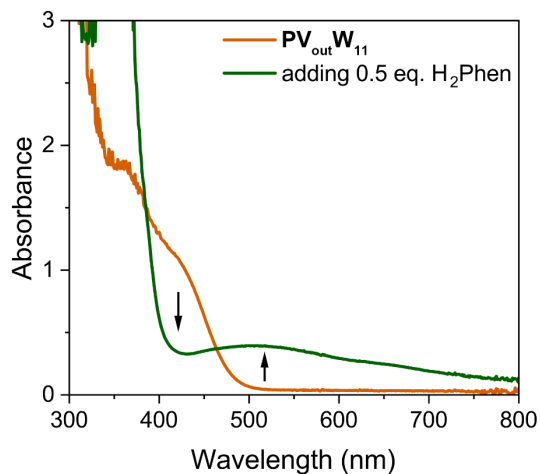


**Figure S17.** Electronic absorption spectra of 0.5 mM  $PV_{out}W_{11}$  after adding half equivalent of  $H_2Phen$ .

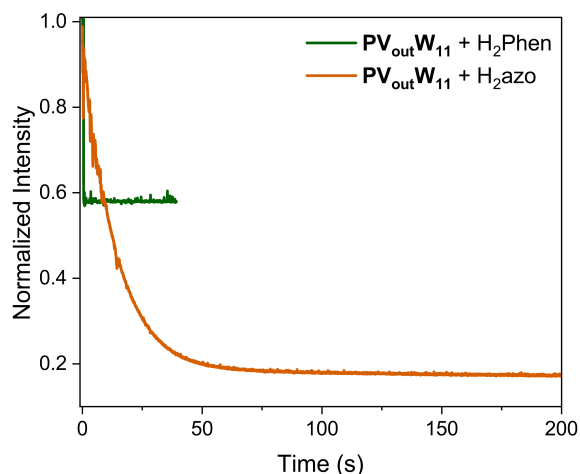


**Figure S18.** Normalized absorbance trace over time of 0.25 mM  $\text{PV}_{\text{out}}\text{W}_{11}$  after the addition of 2.5 mM (green)  $\text{H}_2\text{Phen}$  or (orange)  $\text{H}_2\text{Azo}$  at  $-30^\circ\text{C}$ . The monitored wavelengths are 424 and 370 nm for the addition of  $\text{H}_2\text{Phen}$  and  $\text{H}_2\text{Azo}$ , respectively. The discrepancy in the absorbance change of  $\text{PV}_{\text{out}}\text{W}_{11}$  towards  $\text{H}_2\text{Phen}$  and  $\text{H}_2\text{Azo}$  originates from the different monitored wavelengths to avoid the overlapped absorption. The full electronic absorption spectra are shown in Figure 5a, S24.

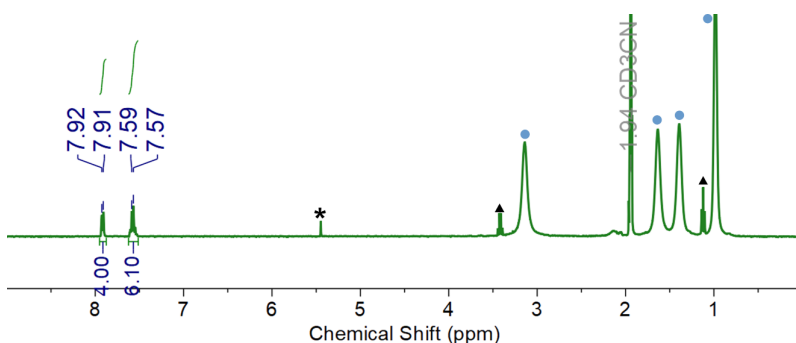


**Figure S19.**  $^1\text{H-NMR}$  spectrum of  $\text{PV}_{\text{out}}\text{W}_{11}$  after adding half equivalent of hydrazobenzene ( $\text{H}_2\text{azo}$ ), showing the complete conversion to azobenzene. The blue circles represent the  $[\text{Bu}_4\text{N}]^+$  cations in the cluster, the black triangles are diethyl ether, and the asterisk is the trace unidentified impurity.

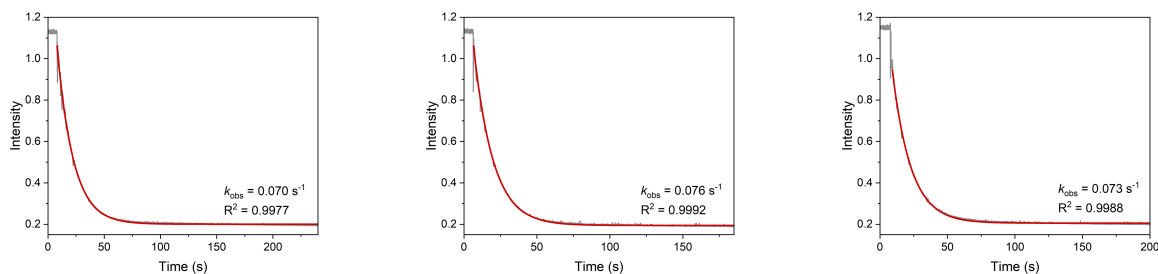


**Figure S20.** Plot of absorbance at 370 nm over time (s) for the reactions between 0.25 mM  $\text{PV}_{\text{out}}\text{W}_{11}$  and 2.5 mM  $\text{H}_2\text{Azo}$  under pseudo-1<sup>st</sup>-order condition in MeCN at  $-30^\circ\text{C}$  with (gray) raw data and (red) fitting curve, along with fir-derived  $k_{\text{obs}}$  and  $R^2$  parameters.

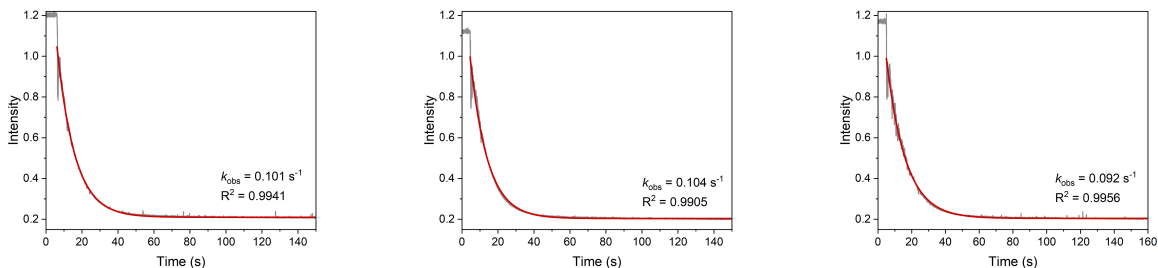


**Figure S21.** Plot of absorbance at 370 nm over time for the reactions between 0.25 mM  $PV_{out}W_{11}$  and 3 mM  $H_2Azo$  under pseudo-1<sup>st</sup>-order condition in MeCN at  $-30\text{ }^\circ\text{C}$  with (gray) raw data and (red) fitting curve, along with fir-derived  $k_{obs}$  and  $R^2$  parameters.

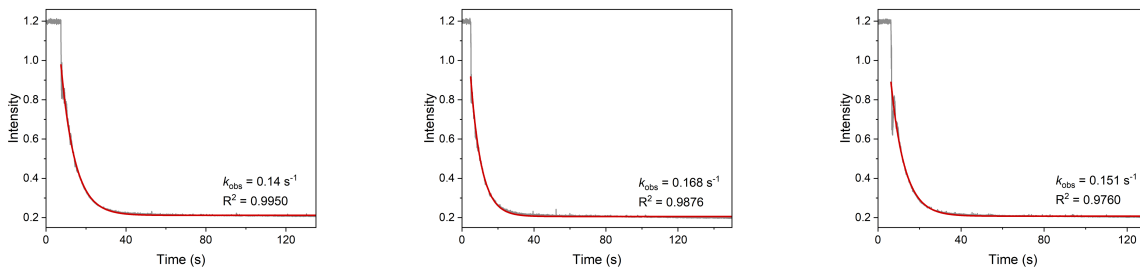


**Figure S22.** Plot of absorbance at 370 nm over time for the reactions between 0.25 mM  $PV_{out}W_{11}$  and 4 mM  $H_2Azo$  under pseudo-1<sup>st</sup>-order condition in MeCN at  $-30\text{ }^\circ\text{C}$  with (gray) raw data and (red) fitting curve, along with fir-derived  $k_{obs}$  and  $R^2$  parameters.

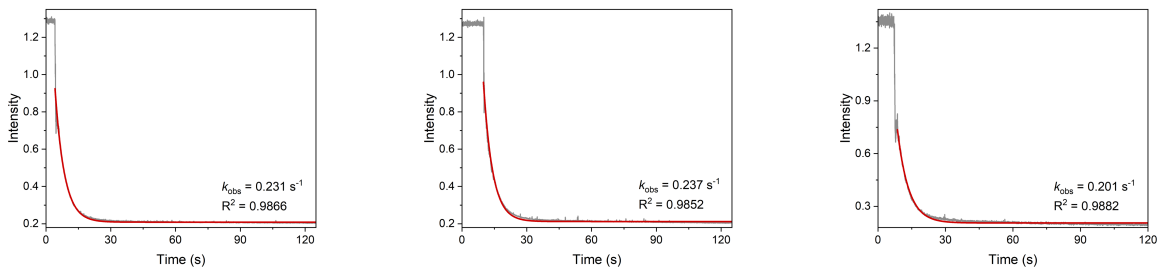


**Figure S23.** Plot of absorbance at 370 nm over time for the reactions between 0.25 mM  $PV_{out}W_{11}$  and 5 mM  $H_2Azo$  under pseudo-1<sup>st</sup>-order condition in MeCN at  $-30\text{ }^\circ\text{C}$  with (gray) raw data and (red) fitting curve, along with fir-derived  $k_{obs}$  and  $R^2$  parameters.

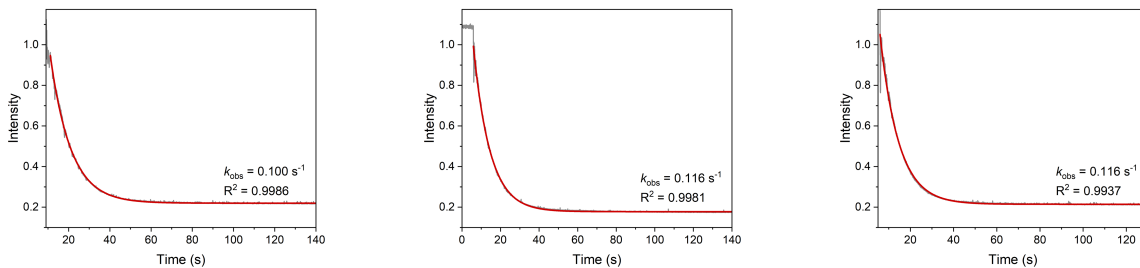


**Figure S24.** Plot of absorbance at 370 nm over time for the reactions between 0.25 mM  $PV_{out}W_{11}$  and 2.5 mM  $H_2Azo$  under pseudo-1<sup>st</sup>-order condition in MeCN at  $-20\text{ }^\circ\text{C}$  with (gray) raw data and (red) fitting curve, along with fir-derived  $k_{obs}$  and  $R^2$  parameters.

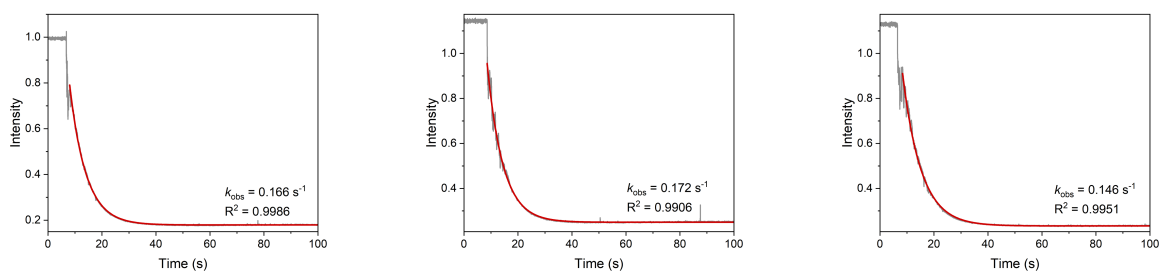


**Figure S25.** Plot of absorbance at 370 nm over time for the reactions between 0.25 mM  $\text{PV}_{\text{out}}\text{W}_{11}$  and 2.5 mM  $\text{H}_2\text{Azo}$  under pseudo-1<sup>st</sup>-order condition in MeCN at  $-10\text{ }^\circ\text{C}$  with (gray) raw data and (red) fitting curve, along with fir-derived  $k_{\text{obs}}$  and  $R^2$  parameters.

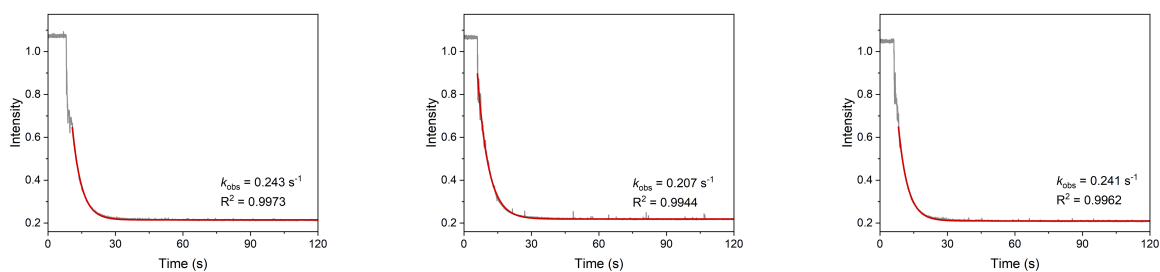


**Figure S26.** Plot of absorbance at 370 nm over time for the reactions between 0.25 mM  $\text{PV}_{\text{out}}\text{W}_{11}$  and 2.5 mM  $\text{H}_2\text{Azo}$  under pseudo-1<sup>st</sup>-order condition in MeCN at  $0\text{ }^\circ\text{C}$  with (gray) raw data and (red) fitting curve, along with fir-derived  $k_{\text{obs}}$  and  $R^2$  parameters.



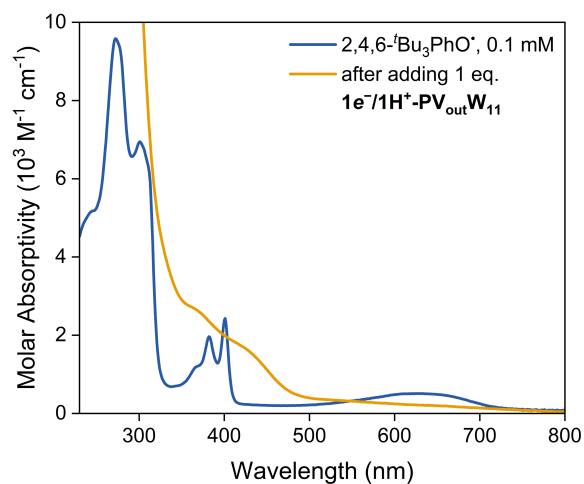


**Figure S27.** Electronic absorption spectra of (blue) 0.1 mM 2,4,6- $\text{Bu}_3\text{PhO}^\bullet$  radical in acetonitrile and (yellow) after the addition of one equivalent of  $1e^-/1\text{H}^+-\text{PV}_{\text{out}}\text{W}_{11}$ , showing the disappearance of 2,4,6- $\text{Bu}_3\text{PhO}^\bullet$  radical and emergence of fully-oxidized  $\text{PV}_{\text{out}}\text{W}_{11}$ .

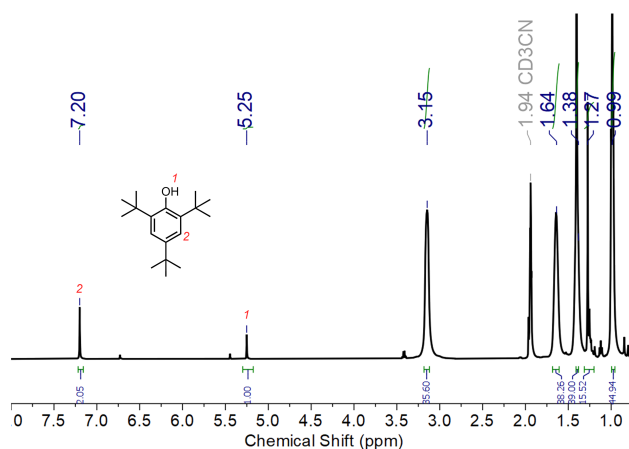


**Figure S28.** NMR spectrum of stoichiometric mixture of 2,4,6- $\text{Bu}_3\text{PhO}^\bullet$  radical and  $1e^-/1\text{H}^+-\text{PV}_{\text{out}}\text{W}_{11}$  in  $\text{CD}_3\text{CN}$ , showing the existence of  $-\text{OH}$  signal of 2,4,6- $\text{Bu}_3\text{PhOH}$ .

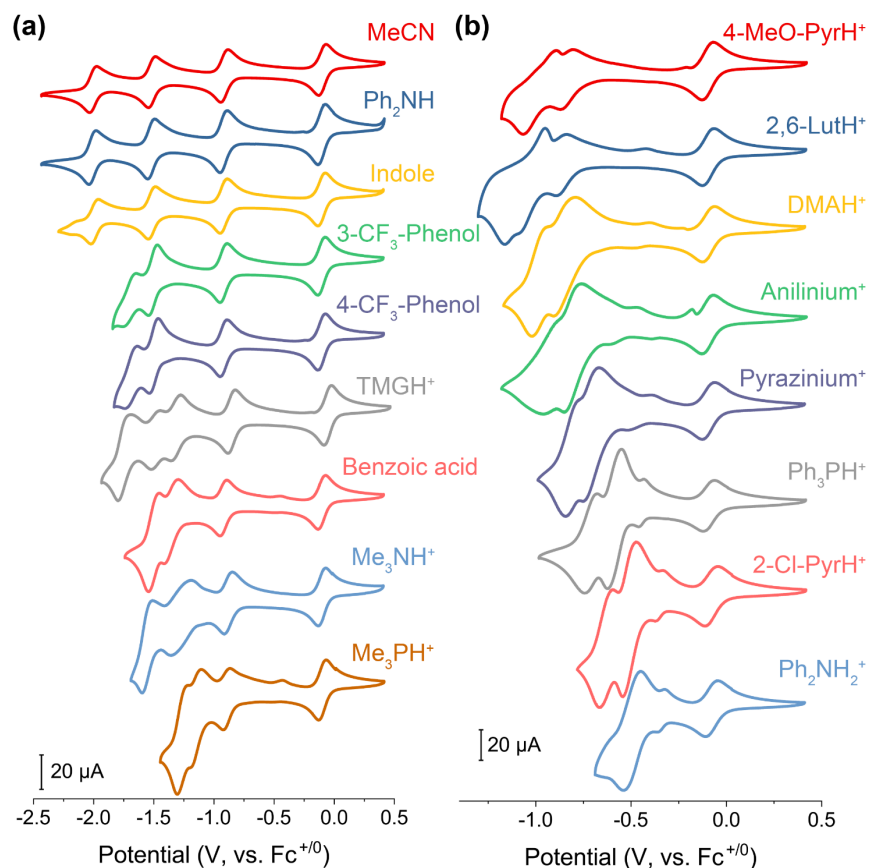


**Figure S29.** Cyclic voltammograms of 1 mM  $V_{in}W_{12}$  obtained in acetonitrile in the presence of 4 mM various organic acids with the scan rate of 100 mV/s, using 0.1 M  $[nBu_4N]PF_6$  as the supporting electrolyte. Ferrocene is used for each measurement as the internal standard. The corresponding acids are listed in **Table S1**.

Note: the errors in  $pK_a$  and resulting BDFE are predicted by linear regression analysis in adoption of 95% confidence level of the calculated confidence intervals.

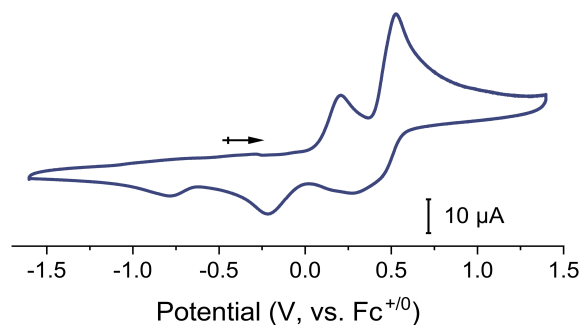


**Figure S30.** Cyclic voltammograms of 1 mM 1,4-dihydroxynaphthalene ( $\text{H}_2\text{NQ}$ ) in acetonitrile with the scan rate of 100 mV/s, using 0.1 M  $[\text{nBu}_4\text{N}]\text{PF}_6$  as the supporting electrolyte.

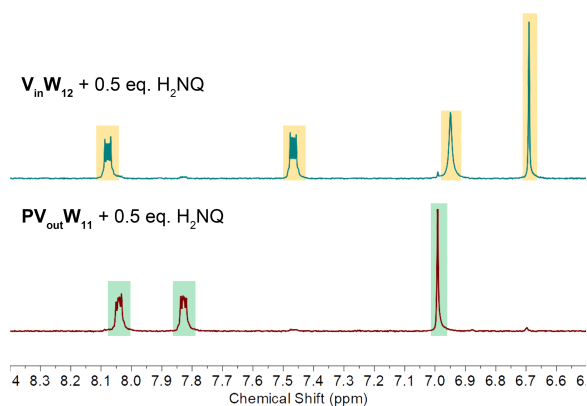


**Figure S31.**  $^1\text{H}$  NMR spectra of the mixture of (upper)  $\text{V}_{\text{in}}\text{W}_{12}$  and half equivalent of 1,4-dihydroxynaphthalene ( $\text{H}_2\text{NQ}$ ) and (lower)  $\text{PV}_{\text{out}}\text{W}_{11}$  and  $\text{H}_2\text{NQ}$  in  $\text{CD}_3\text{CN}$ . The yellow- and green-shaded areas represent the  $\text{H}_2\text{NQ}$  and dehydrogenated product 1,4-naphthoquinone (NQ), respectively.

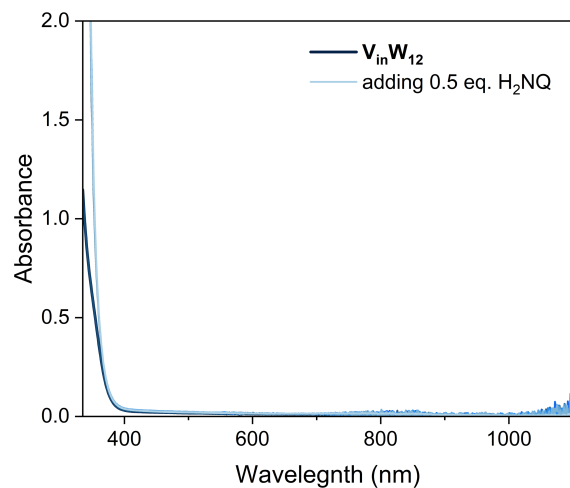


**Figure S32.** Electronic absorption spectra of 0.5 mM  $V_{in}W_{12}$  after adding half equivalent of  $H_2NQ$ .

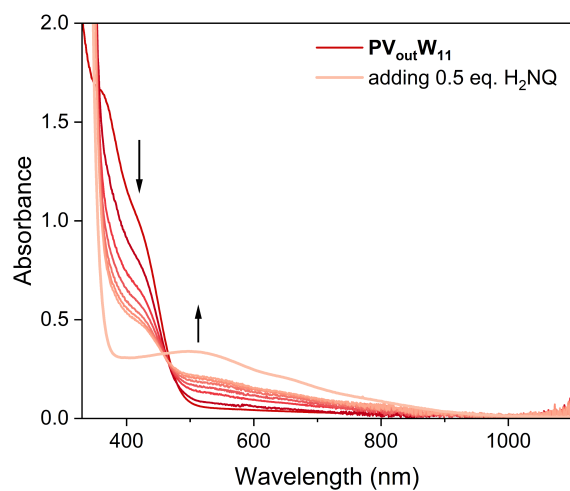


**Figure S33.** Electronic absorption spectra of 0.5 mM  $PV_{out}W_{11}$  after adding half equivalent of  $H_2NQ$ .

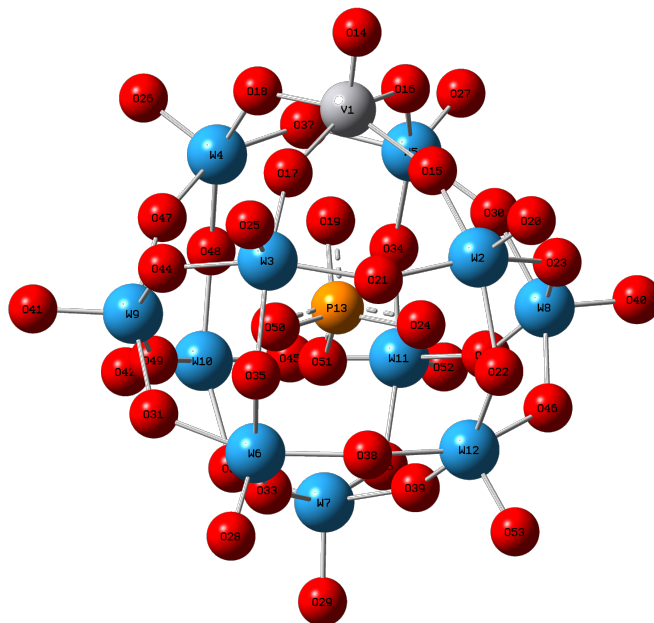


**Figure S34.** Illustration of atom numbers of  $PV_{out}W_{11}$  in conceptual density functional theory (CDFT) calculation.

**Table S2.** Conceptual density functional theory (CDFT) results for **PV<sub>out</sub>W<sub>11</sub>**.

Atom	Electrophilicity index (e*eV)	Nucleophilicity index (e*eV)	Local hyper-softness, $s^2(r)$ (e/Hartree <sup>2</sup> )
1(V)	0.143	0.091	2.67
2(W)	0.030	0.199	0.25
3(W)	0.030	0.152	0.33
4(W)	0.032	0.151	0.36
5(W)	0.032	0.186	0.30
6(W)	0.012	0.117	0.03
7(W)	0.011	0.112	0.01
8(W)	0.016	0.151	0.05
9(W)	0.016	0.122	0.10
10(W)	0.012	0.118	0.03
11(W)	0.012	0.131	0.01
12(W)	0.012	0.134	0.00
13(P)	-0.001	-0.021	0.02
14(O)	0.105	0.356	1.43
15(O)	-0.004	0.666	-1.27
16(O)	0.010	0.861	-1.35
17(O)	-0.004	0.035	-0.14
18(O)	0.010	0.118	-0.02
19(O)	-0.007	-0.048	-0.05
20(O)	0.030	0.385	-0.10
21(O)	0.015	0.179	-0.03
22(O)	0.008	0.094	-0.02
23(O)	0.007	0.562	-0.86
24(O)	-0.001	-0.034	0.05
25(O)	0.030	0.293	0.07
26(O)	0.034	0.311	0.11
27(O)	0.034	0.390	-0.03
28(O)	0.023	0.265	-0.01
29(O)	0.022	0.259	-0.04
30(O)	0.001	0.437	-0.75
31(O)	0.010	0.147	-0.06
32(O)	0.008	0.123	-0.06
33(O)	0.003	0.058	-0.04
34(O)	0.003	0.054	-0.04
35(O)	0.008	0.115	-0.05
36(O)	0.008	0.119	-0.05
37(O)	0.021	0.200	0.05
38(O)	0.002	0.041	-0.04
39(O)	0.003	0.047	-0.03
40(O)	0.025	0.352	-0.14
41(O)	0.025	0.269	0.01
42(O)	0.022	0.263	-0.03
43(O)	0.006	0.112	-0.08
44(O)	0.007	0.136	-0.10
45(O)	0.007	0.106	-0.05
46(O)	0.010	0.159	-0.08
47(O)	0.001	0.082	-0.12

---

48(O)	0.003	0.056	-0.05
49(O)	0.006	0.100	-0.06
50(O)	-0.001	0.008	-0.03
51(O)	0.002	0.013	0.01
52(O)	0.022	0.274	-0.05
53(O)	0.023	0.292	-0.06

---

## References

1. M. J. Frisch, G. W. Trucks, H. B. Schlegel, G. E. Scuseria, M. A. Robb, J. R. Cheeseman, G. Scalmani, V. Barone, G. A. Petersson, H. Nakatsuji, X. Li, M. Caricato, A. V. Marenich, J. Bloino, B. G. Janesko, R. Gomperts, B. Mennucci, H. P. Hratchian, J. V. Ortiz, A. F. Izmaylov, J. L. Sonnenberg, D. Williams-Young, F. Ding, F. Lipparini, F. Egidi, J. Goings, B. Peng, A. Petrone, T. Henderson, D. Ranasinghe, V. G. Zakrzewski, J. Gao, N. Rega, G. Zheng, W. Liang, M. Hada, M. Ehara, K. Toyato, R. Fukuda, J. Hasegawa, M. Ishida, T. Nakajima, Y. Honda, O. Kitao, H. Nakai, T. Vreven, K. Throssell, J. A. Montgomery Jr., J. E. Peralta, F. Ogliaro, M. J. Bearpark, J. J. Heyd, E. N. Brothers, K. N. Kudin, V. N. Staroverov, T. A. Keith, R. Kobayashi, J. Normand, K. Raghavachari, A. P. Rendell, J. C. Burant, S. S. Iyengar, J. Tomasi, M. Cossi, J. M. Millam, M. Klene, C. Adamo, R. Cammi, J. W. Ochterski, R. L. Martin, K. Morokuma, O. Farkas, J. B. Foresman and D. J. Fox, *Gaussian 16*, 2016.
2. H. S. Yu, X. He, S. L. Li and D. G. Truhlar, *Chem. Sci.*, 2016, **7**, 5032–5051.
3. F. Weigend and R. Ahlrichs, *Phys. Chem. Chem. Phys.*, 2005, **7**, 3297–3305.
4. T. Lu, *J. Chem. Phys.*, 2024, **161**, 082503.
5. T. Lu and F. Chen, *J. Comput. Chem.*, 2012, **33**, 580–592.
6. T. Lu and Q. Chen, in *Conceptual Density Functional Theory: Towards a New Chemical Reactivity Theory, Volume 2*, WILEY-VCH GmbH: Weinheim, 2022, pp. 631–647.
7. S. D. Ponja, S. Sathasivam, H. O. Davies, I. P. Parkin and C. J. Carmalt, *ChemPlusChem*, 2016, **81**, 307–314.
8. S. Himeno, M. Takamoto, A. Higuchi and M. Maekawa, *Inorg. Chim. Acta*, 2003, **348**, 57–62.
9. H.-Z. Yu, Y.-M. Yang, L. Zhang, Z.-M. Dang and G.-H. Hu, *J. Phys. Chem. A*, 2014, **118**, 606–622.
10. F. G. Bordwell, J. C. Branca, J. E. Bares and R. Filler, *J. Org. Chem.*, 1988, **53**, 780–782.
11. F. Maran, D. Celadon, M. G. Severin and E. Vianello, *J. Am. Chem. Soc.*, 1991, **113**, 9320–9329.
12. A. Kütt, S. Tshepelevitsh, J. Saame, M. Lõkov, I. Kaljurand, S. Selberg and I. Leito, *Eur. J. Org. Chem.*, 2021, **2021**, 1407–1419.
13. S. Tshepelevitsh, A. Kütt, M. Lõkov, I. Kaljurand, J. Saame, A. Heering, P. G. Pliieger, R. Vianello and I. Leito, *Eur. J. Org. Chem.*, 2019, **2019**, 6735–6748.
14. M. Vallaro, G. Ermondi, J. Saame, I. Leito and G. Caron, *Bioorg. Med. Chem.*, 2023, **81**, 117203.